

University of Groningen

Efficient Selective Sorting of Semiconducting Carbon Nanotubes Using Ultra-Narrow-Band-Gap Polymers

Talsma, Wytse; Ye, Gang; Liu, Yuru; Duim, Herman; Dijkstra, Sietske; Tran, Karolina; Qu, Junle; Song, Jun; Chiechi, Ryan C.; Loi, Maria Antonietta

Published in:
ACS Applied Materials and Interfaces

DOI:
[10.1021/acsami.2c07158](https://doi.org/10.1021/acsami.2c07158)

IMPORTANT NOTE: You are advised to consult the publisher's version (publisher's PDF) if you wish to cite from it. Please check the document version below.

Document Version
Publisher's PDF, also known as Version of record

Publication date:
2022

[Link to publication in University of Groningen/UMCG research database](#)

Citation for published version (APA):

Talsma, W., Ye, G., Liu, Y., Duim, H., Dijkstra, S., Tran, K., Qu, J., Song, J., Chiechi, R. C., & Loi, M. A. (2022). Efficient Selective Sorting of Semiconducting Carbon Nanotubes Using Ultra-Narrow-Band-Gap Polymers. *ACS Applied Materials and Interfaces*, 14(33), 38056-38066.
<https://doi.org/10.1021/acsami.2c07158>

Copyright

Other than for strictly personal use, it is not permitted to download or to forward/distribute the text or part of it without the consent of the author(s) and/or copyright holder(s), unless the work is under an open content license (like Creative Commons).

The publication may also be distributed here under the terms of Article 25fa of the Dutch Copyright Act, indicated by the "Taverne" license. More information can be found on the University of Groningen website: <https://www.rug.nl/library/open-access/self-archiving-pure/taverne-amendment>.

Take-down policy

If you believe that this document breaches copyright please contact us providing details, and we will remove access to the work immediately and investigate your claim.

Efficient Selective Sorting of Semiconducting Carbon Nanotubes Using Ultra-Narrow-Band-Gap Polymers

Wytse Talsma,[†] Gang Ye,^{*,†} Yuru Liu, Herman Duim, Sietske Dijkstra, Karolina Tran, Junle Qu, Jun Song, Ryan C. Chiechi,^{*} and Maria Antonietta Loi^{*}



Cite This: *ACS Appl. Mater. Interfaces* 2022, 14, 38056–38066



Read Online

ACCESS |

Metrics & More

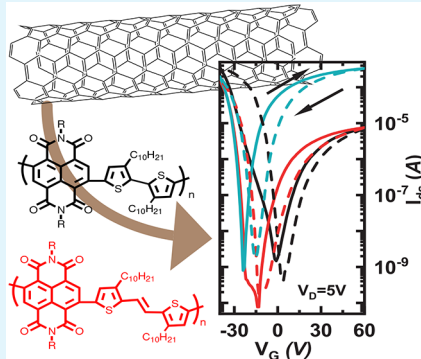


Article Recommendations



Supporting Information

ABSTRACT: Conjugated polymers with narrow band gaps are particularly useful for sorting and discriminating single-walled carbon nanotubes (s-SWCNT) due to the low charge carrier injection barrier for transport. In this paper, we report two newly synthesized narrow-band-gap conjugated polymers (PNDITEG-TVT and PNDIC8TEG-TVT) based on naphthalene diimide (NDI) and thienylenevinylene (TVT) building blocks, decorated with different polar side chains that can be used for dispersing and discriminating s-SWCNT. Compared with the mid-band-gap conjugated polymer PNDITEG-AH, which is composed of naphthalene diimide (NDI) and head-to-head bithiophene building blocks, the addition of a vinylene linker eliminates the steric congestion present in head-to-head bithiophene, which promotes backbone planarity, extending the π -conjugation length and narrowing the band gap. Cyclic voltammetry (CV) and density functional theory (DFT) calculations suggest that inserting a vinylene group in a head-to-head bithiophene efficiently lifts the highest occupied molecular orbital (HOMO) level (-5.60 eV for PNDITEG-AH, -5.02 eV for PNDITEG-TVT, and -5.09 eV for PNDIC8TEG-TVT). All three polymers are able to select for s-SWCNT, as evidenced by the sharp transitions in the absorption spectra. Field-effect transistors (FETs) fabricated with the polymer:SWCNT inks display p-dominant properties, with higher hole mobilities when using the NDI-TVT polymers as compared with PNDITEG-AH ($0.6\text{ cm}^2\text{ V}^{-1}\text{ s}^{-1}$ for HiPCO:PNDITEG-AH, $1.5\text{ cm}^2\text{ V}^{-1}\text{ s}^{-1}$ for HiPCO:PNDITEG-TVT, and $2.3\text{ cm}^2\text{ V}^{-1}\text{ s}^{-1}$ for HiPCO:PNDIC8TEG-TVT). This improvement is due to the better alignment of the HOMO level of PNDITEG-TVT and PNDIC8TEG-TVT with that of the dominant SWCNT specie.



KEYWORDS: low-band-gap conjugated polymers, polar side chain, SWCNT FET, sorting SWCNTs, polymer wrapping

INTRODUCTION

Single-walled carbon nanotubes (SWCNT) are one of the most promising next-generation electronic materials for field-effect transistors (FETs),^{1–5} logic circuits,^{6–10} sensors,^{11,12} flexible electronics,^{13–15} microprocessors,^{16,17} and other applications.^{18–21} Among these applications, FETs based on semiconducting SWCNT (s-SWCNT) are attractive because of their high charge carrier mobility, low dimensionality, and the possibility for high-density integration and low-cost solution processability.^{22–24} Indeed, pure s-SWCNT FETs have demonstrated performance superior to that of silicon.²⁵ However, as-synthesized SWCNT are a mixture of roughly 2:1 s-SWCNT and m-SWCNT (metallic SWCNT), which limits their application in devices.^{26,27}

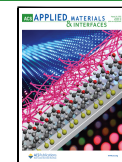
To overcome these issues, several approaches to isolate pure s/m-SWCNT have been developed. Among these are (i) density gradient ultracentrifugation (DGU),²⁸ (ii) size-exclusion chromatography methods,²⁹ and (iii) noncovalent selective sorting of s-SWCNT by conjugated polymers.^{22–24} The latter technique has received significant attention because of its high dispersion efficiency, selectivity, and low cost.²⁷

Since the pioneering work of Nish et al. in 2007, where polyfluorene was used to select semiconducting carbon nanotubes at a low concentration,³⁰ many conjugated polymers able to disperse and sort s-SWCNT selectively have been reported.^{22,27} Most of those conjugated polymers are fluorene-,^{30,31} carbazole-,^{32,33} and thiophene-based polymers,^{34,35} with a highest occupied molecular orbital (HOMO) and lowest unoccupied molecular orbital (LUMO) separation (band gap) of about 2 or 3 eV (see Figure 1a).^{23,24,27} From the perspective of device fabrication, the advantage of using conjugated polymers to wrap s-SWCNT selectively is that the noncovalently bound polymers do not necessarily affect the intrinsic charge transport of the SWCNT. However, in practice, polymers with relatively large band gaps

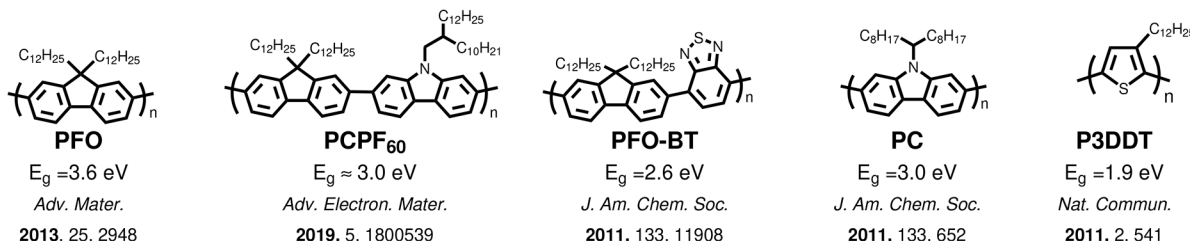
Received: April 22, 2022

Accepted: July 28, 2022

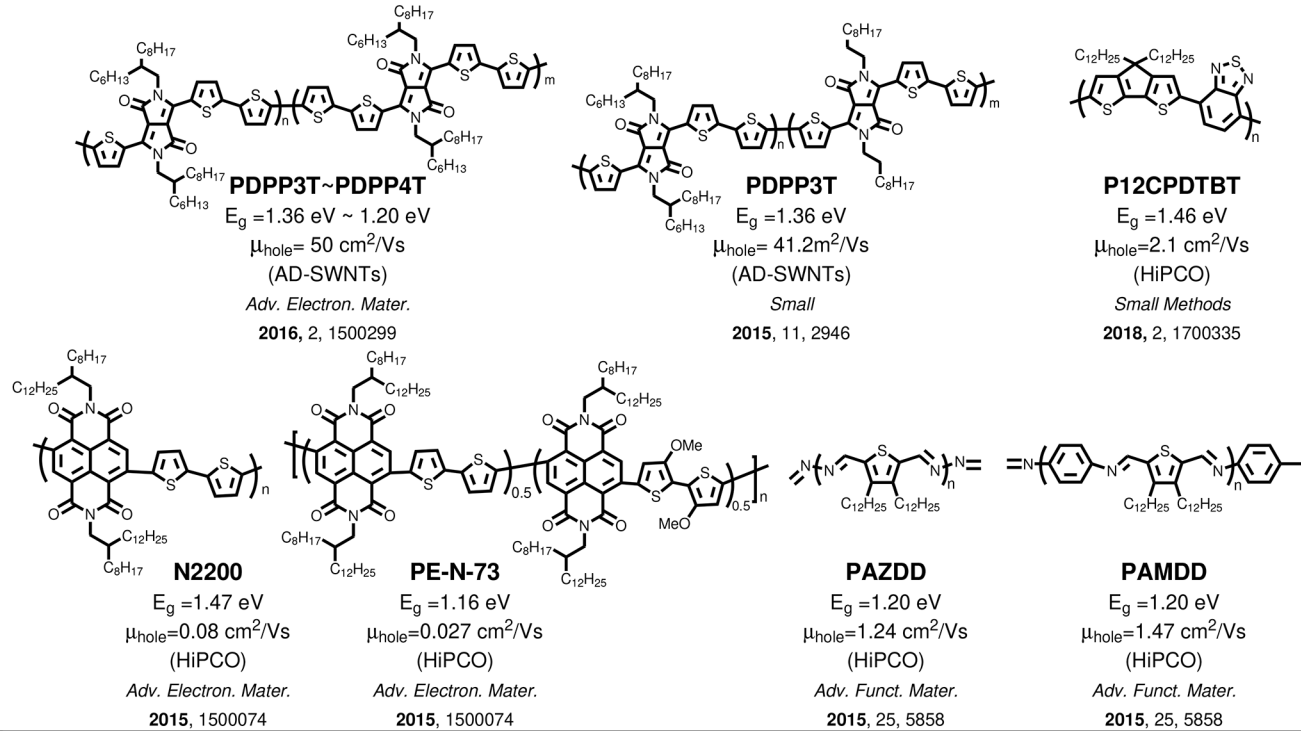
Published: August 9, 2022



(a) Wide- or mid-band-gap conjugated polymers for wrapping SWCNT



(b) Narrow-band-gap conjugated polymers for wrapping SWCNT



(c)

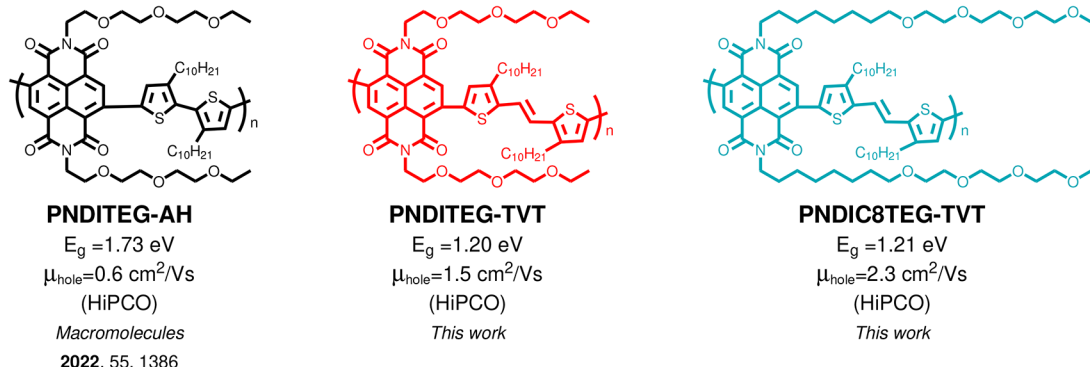


Figure 1. Chemical structures of (a) representative wide- or mid-band-gap conjugated polymers for selecting and sorting SWCNTs reported in the literature and (b) narrow-band-gap conjugated polymers for selecting and sorting SWCNTs reported so far. The mentioned mobilities are for s-SWCNT FETs (c) naphthalene diimide based low-band-gap conjugated polymers presented in this work.^{31,33,34,36–41,53}

create energetic barriers to intertube transport in the solid state, deleteriously affecting the electrical performance of devices. This barrier is the result of an energy mismatch between the s-SWCNT and the polymer; thus, to reduce the energetic barrier between the polymer and nanotubes, the band energies (HOMO/LUMO levels) of the wrapping polymer need to match those of the s-SWCNT. While there are some instances in which it might be desirable to promote

hole or electron transport, narrow-band-gap polymers match both levels, facilitating both electron and hole transport, making the s-SWCNT networks more generalizable to device applications.

There are few examples of narrow-band-gap conjugated polymers that demonstrably disperse SWCNT selectively (see Figure 1b).^{36–40} In our previous work, we showed that the naphthalene-diimide (NDI) based, donor–acceptor (D–A),

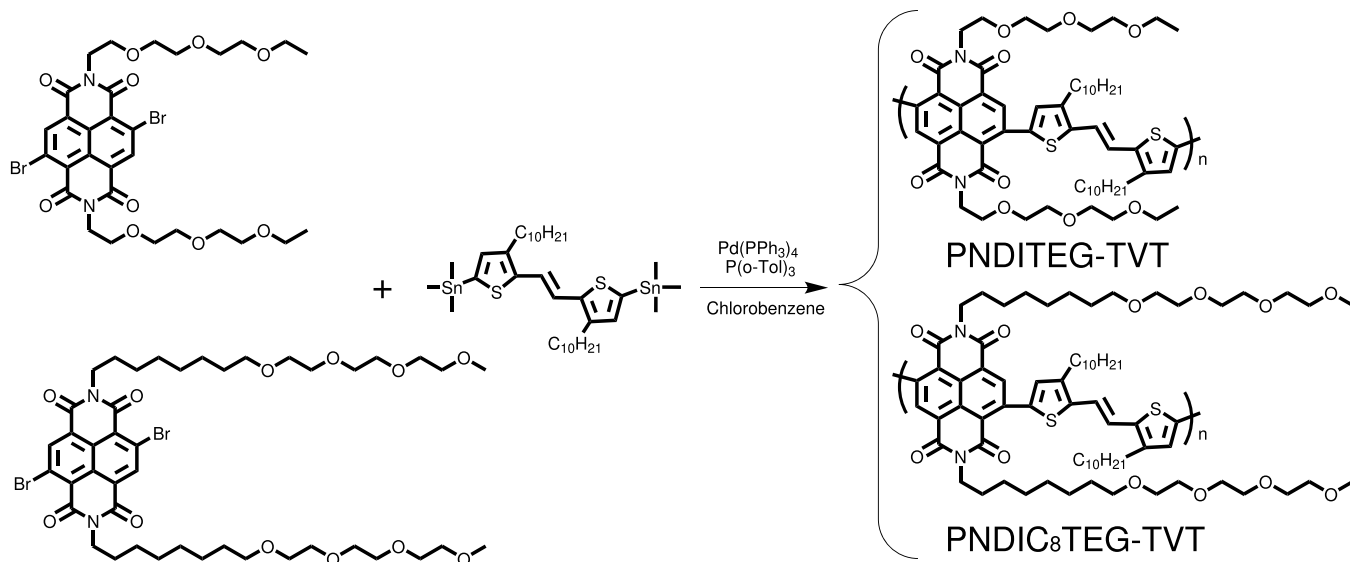


Figure 2. Synthesis routes to naphthalene diimide and thienylennevinylene based low-band-gap conjugated polymers PNDITEG-TVT and PNDIC₈TEG-TVT, used in this work.

narrow-band-gap conjugated polymers N2200 (1.46 eV) and PE-N-73 (1.16 eV) dispersed HiPCO SWCNTs. However, due to the weak interaction with SWCNTs, the yield was limited, resulting in inks of low concentration.³⁹ Because of the low concentration of the tested solution, FETs made from these inks did not perform as well as other polymers (e.g. P3DDT and PFO). Encouragingly, the HOMO level of PE-N-73 is better aligned with that of s-SWCNTs, resulting in reduced IV hysteresis.^{1,39} That work motivated us to design new narrow-band-gap conjugated polymers that maximize interactions with SWCNTs to disperse and select s-SWCNTs.

Very recently, we addressed the weak interaction between D–A conjugated polymers and SWCNTs by introducing polar triethylene glycol side chains on the D–A conjugated polymer backbone. We demonstrated the wrapping ability of the mid-band-gap, D–A conjugated polymer (**PNDITEG-AH**), comprising NDI and head-to-head bithiophene, which is significantly improved by including polar triethylene glycol side chains as compared to alkyl side chains.⁴¹ For this work, we partly make use of the same data set regarding this specific polymer (**PNDITEG-AH**) and thereon-based devices.

Inspired by these results, we developed new NDI-based, D–A, narrow-band-gap conjugated polymers, **PNDITEG-TVT** and **PNDIC₈TEG-TVT**, which include a vinylene linker between the head-to-head bithiophene moiety of the **PNDITEG-AH** backbone to increase the effective conjugation length by planarizing the backbone, with the goal of promoting intertube transport in the resulting inks. It has been reported that backbone planarity and the aromatic surface area of the polymer promote better π – π interactions with SWCNT, thus enhancing the s-SWCNT wrapping capability.^{37,38} Importantly, **PNDITEG-TVT** and **PNDIC₈TEG-TVT** remain flexible due to the steric hindrance of the NDI with the adjacent thiophene, thus avoiding the formation of a rigid conjugated polymer backbone that would disfavor the wrapping process energetically, reducing the yield for the selection of s-SWCNTs.⁴⁰

In this paper, we describe the design and synthesis of two narrow-band-gap conjugated polymers by copolymerization of NDI moieties with thienylennevinylene (TVT) decorated with polar side chain for dispersing and discriminating s-SWCNTs.

Both polymers demonstrate the capacity of selectively dispersing s-SWCNTs in good yields. Absorption measurements of the resulting inks reveal that **PNDITEG-AH** exhibits the highest yield for s-SWCNTs dispersion due to higher flexibility of the backbone, while the planar structure of **PNDITEG-TVT** leads to a modest decrease of 12% in dispersion ability. FETs fabricated from either of these polymer-wrapped s-SWCNT inks exhibit excellent charge-transport properties due to narrow band gap lowering the energetic barrier for intertube charge-transport. This work clearly demonstrates the critical role of backbone flexibility and planarity, affording a deeper understanding of the relationship between polymer structure and the wrapping and selecting of s-SWCNTs.

RESULTS AND DISCUSSION

Synthesis and Characterization. The synthesis routes and chemical structures of the two new conjugated polymers that were used to study the dispersion and discrimination of semiconducting carbon nanotubes are shown in Figure 2. The synthesis of **PNDITEG-AH** was carried out according to literature procedures.⁴¹ The monomers were synthesized and purified according to published procedures with slight modifications (see the Supporting Information for details).^{42–44} Both polymers were synthesized by a typical palladium-catalyzed Stille polycondensation of symmetrical dibromo naphthalene diimide and distannyl thienylennevinylene monomers. Polymers were obtained by refluxing the degassed polymerization mixture for 3 days. After polymerization, the crude polymers were collected by precipitation in methanol. Impurities and low-molecular-weight fractions were removed by continuous extraction with methanol followed by hexane and then chloroform in a Soxhlet extractor. Finally, the polymer solution in chloroform was concentrated, redissolved, precipitated into cold methanol, collected, and dried in vacuum. The yields for **PNDITEG-AH**, **PNDITEG-TVT**, and **PNDIC₈TEG-TVT** are 74, 87, and 90%, respectively. The target conjugated polymer structures were characterized by ¹H NMR, FT-IR, MALDI-TOF-MS, and GPC (Figures S16–S21 and S23–S25 and Table S1). The thermal properties of these

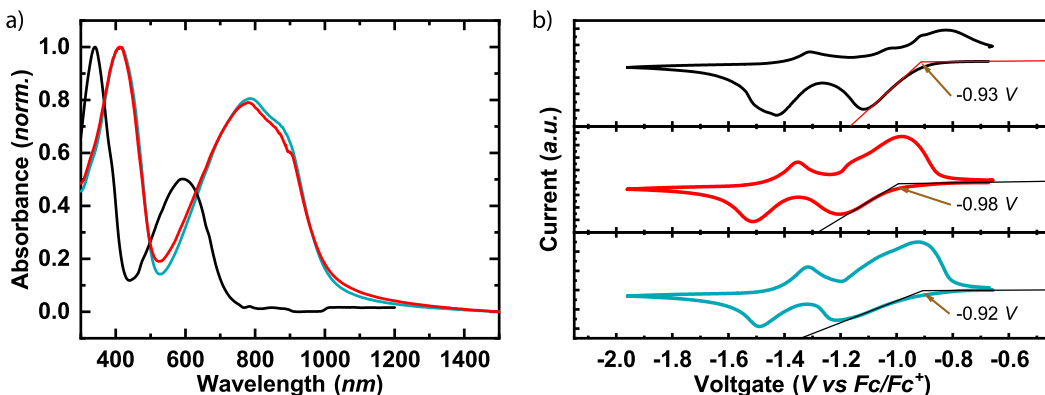


Figure 3. (a) Normalized absorption spectra of pristine PNDITEG-AH (black), PNDITEG-TVT (red), and PNDIC8TEG-TVT (turquoise) as drop-cast (from CHCl_3) films. (b) Cyclic voltammograms of thin films of PNDITEG-AH (black), PNDITEG-TVT (red), and PNDIC8TEG-TVT (turquoise) versus Fc/Fc^+ on a glassy carbon working electrode immersed in 0.1 mol L^{-1} $n\text{-Bu}_4\text{NPF}_6$ acetonitrile solution at 100 m V s^{-1} .

three polymers were evaluated by thermogravimetric analysis (TGA) and differential scanning calorimetry (DSC). The temperature of 5% weight-loss was selected as the onset point of decomposition (T_d). As shown in Figure S26 a, all the polymers show excellent stability with a decomposition temperature of 361°C for PNDITEG-AH, 373°C for PNDITEG-TVT, and 407°C for PNDIC8TEG-TVT. The DSC curves of PNDITEG-TVT and PNDIC8TEG-TVT reveal no distinct phase transition from room temperature to 300°C , while PNDITEG-AH shows a melting transition at 239°C in the second heating cycle (Figure S26 b).

Optical and Electrochemical Properties. Figure 3a shows the absorption spectra of thin films of PNDITEG-AH, PNDITEG-TVT, and PNDIC8TEG-TVT. All these polymers show two distinct absorption bands that can be assigned to the high energy $\pi-\pi^*$ transition (300–400 nm for PNDITEG-AH, 300–500 nm for PNDITEG-TVT and PNDIC8TEG-TVT) and the broad, low-energy intramolecular charge-transfer transition (400–700 nm for PNDITEG-AH, 550–1000 nm for PNDITEG-TVT and PNDIC8TEG-TVT) originating from its donor–acceptor structure.⁴² PNDITEG-TVT and PNDIC8TEG-TVT have almost identical spectra due to their shared backbone structure, with only subtle changes in their side chains. Their spectra are red-shifted about 193 nm with respect to that of PNDITEG-AH, indicating that the insertion of vinylene moieties reduces the steric hindrance of the head-to-head bithiophene units, promoting backbone planarity and extending the π -conjugation length.^{43–50} The absorption onsets ($\lambda_{\text{onset}}^{\text{film}}$) in films of PNDITEG-AH, PNDITEG-TVT, and PNDIC8TEG-TVT are 718, 1035, and 1020 nm, and their corresponding optical band gap are calculated to be 1.73, 1.20, and 1.21 eV, respectively (see Table 1).

We determined the energy levels of PNDITEG-AH, PNDITEG-TVT and PNDIC8TEG-TVT by cyclic voltammetry (CV); details can be found in the Supporting Information. The results are shown in Figure 3b and summarized in Table 1. All polymers exhibit two quasi-reversible reduction waves, corresponding to n-doping (reduction) as a result of the electron-deficient nature of the NDI moieties. The onset reduction potentials ($E_{\text{onset}}^{\text{Red}}$) of PNDITEG-AH, PNDITEG-TVT, and PNDIC8TEG-TVT are -0.93 , -0.98 , and -0.92 V, respectively. The energy levels of the polymers were calculated using the equation $E_{\text{LUMO}} = -(4.80 + E_{\text{onset}}^{\text{Red}})$ eV, where 4.80 represents the

Table 1. Summary of the Photophysical Properties, Electrochemical Properties, Energy Levels, and Molecular Weights of PNDITEG-AH, PNDITEG-TVT, and PNDIC8TEG-TVT

physical property	PNDITEG-AH	PNDITEG-TVT	PNDIC8TEG-TVT
$\lambda_{\text{max}}^{\text{sol}}$ (nm)	335, 560	390, 690	390, 690
$\lambda_{\text{max}}^{\text{film}}$ (nm)	340, 593	411, 783	411, 785
λ_{onset} (nm)	718	1035	1020
$E_g^{\text{opt},a}$ (nm)	1.73	1.20	1.21
$E_{\text{onset}}^{\text{Red}}$ (V)	-0.93	-0.98	-0.92
LUMO (eV) ^b	-3.87	-3.82	-3.88
HOMO (eV) ^c	-5.60	-5.02	-5.09
LUMO (eV) ^d	-3.64	-3.56	-3.48
HOMO (eV) ^d	-6.15	-5.45	-5.41
M_n (g/mol) ^e	9014	14246	15662
M_w (g/mol) ^e	14568	54452	55990
PDI ^e	1.51	3.83	3.57
DP (degrees of polymerization) ^e	9	13	12

^a $E_g^{\text{opt}} = 1240/\lambda_{\text{onset}}^{\text{film}}$. ^bCalculated from CV: $E_{\text{LUMO}} = -(4.80 + E_{\text{onset}}^{\text{Red}})$ eV. ^cCalculated from E_{LUMO} and E_g^{opt} : $E_{\text{HOMO}} = E_{\text{LUMO}} + E_g^{\text{opt}}$. ^dFrom DFT calculations. ^eFrom GPC analysis.

HOMO energy level of ferrocene against vacuum. Accordingly, the LUMO levels of polymers are -3.87 , -3.82 , and -3.88 eV, respectively. On the basis of the optical band gap and LUMO levels, the calculated HOMO levels of PNDITEG-AH, PNDITEG-TVT, and PNDIC8TEG-TVT are -5.60 , -5.02 , and -5.09 eV, respectively. These results reveal that in addition to planarizing the backbone the incorporation of vinylene moieties into the polymer backbone pushes the HOMO level up, which should further facilitate hole transport between the polymer and s-SWCNT.

Density functional theory (DFT) calculations were carried out on model compounds for PNDITEG-AH, PNDITEG-TVT and PNDIC8TEG-TVT to elucidate further the effect of the vinylene linker on the backbone planarity and energy levels of the frontier orbitals at the B3LYP/6-311G(d) level using Gaussian 16.⁵¹ In Figure S29, the molecular orbital distributions for model compounds of PNDITEG-AH, PNDITEG-TVT, and PNDIC8TEG-TVT are shown. All the LUMOs are localized on the central NDI unit. In contrast, the HOMOs are located on the TVT moiety in PNDITEG-TVT and PNDIC8TEG-TVT and on bithiophene in PNDITEG-

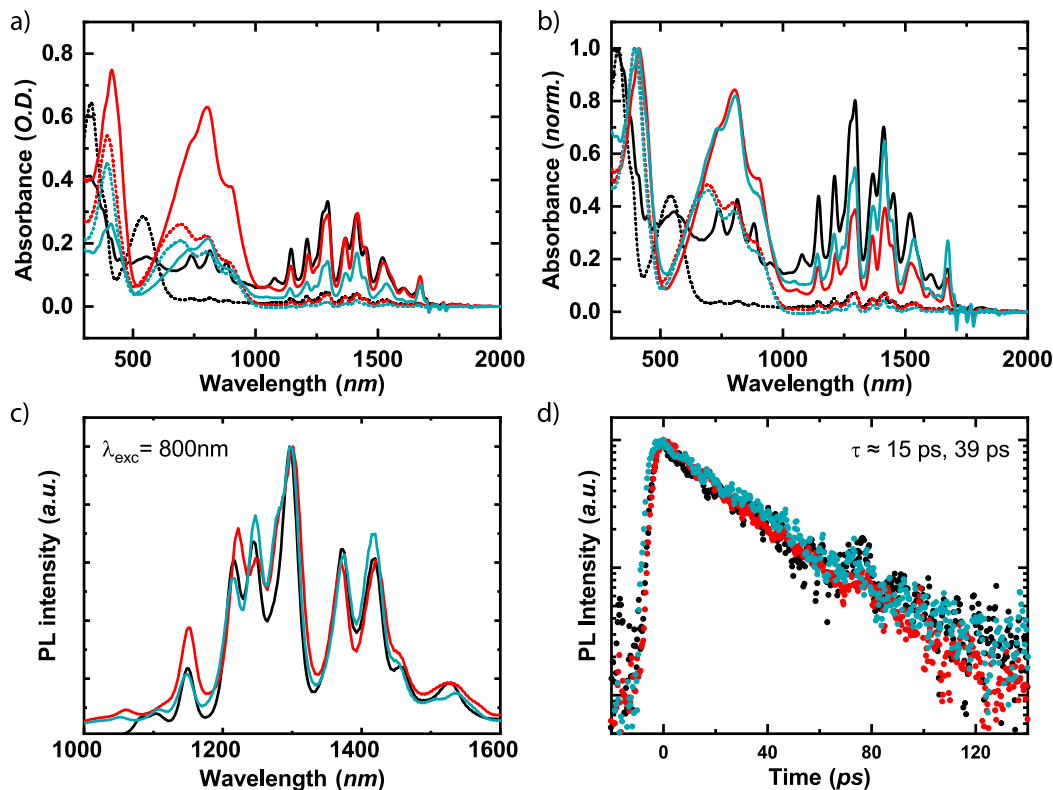


Figure 4. (a) Absorption spectra (in O.D.) of HiPCO:PNDITEG-AH (black), HiPCO:PNDITEG-TVT (red), and HiPCO:PNDIC8TEG-TVT (turquoise) inks as obtained directly from the first discrimination (dotted lines) and after the enrichment procedure (solid lines). (b) Absorption spectra normalized to the free polymer peak. (c) Normalized steady-state photoluminescence of the HiPCO:PNDITEG-AH (black), HiPCO:PNDITEG-TVT (red), and HiPCO:PNDIC8TEG-TVT (turquoise). (d) Photoluminescence decay of the 1140 nm PL peak of the investigated samples. No discernible differences in lifetimes were found between the SWCNT solutions obtained with the different polymers; a fit of the measurements with $I = \sum_{i=1}^2 A_i \exp((-t)/(\tau_i))$ yields lifetimes $\tau_1 = 15$ ps (43%) and $\tau_2 = 39$ ps (57%).

AH. Figure S30 shows that the calculated energy gaps of PNDITEG-TVT and PNDIC8TEG-TVT are lower than that of PNDITEG-AH, which is consistent with the optical band gap results. Interestingly, the introduction of vinylene linker into the head-to-head bithiophene significantly increased the HOMO energy, with little change in the LUMO energy, resulting in a decreased band gap. This is in agreement with our CV measurements.

The dihedral angle between thiophene and thiophene in PNDITEG-AH is 109.0°, which is considerably larger than that of the thiophene adjacent to the vinylene moieties in PNDITEG-TVT (4.8 and 1.7°) and PNDIC8TEG-TVT (4.7 and 1.6°). In addition, the dihedral angle between the NDI unit and adjacent thiophene is also reduced, from 61.9° for PNDITEG-AH to 39.5° for PNDITEG-TVT and to 40.1° for PNDIC8TEG-TVT (see Figures S31–S33 and Table S2).

s-SWCNT Ink Characterization. Having established that inserting a vinylene linker can improve planarity and raise the HOMO level of narrow-band-gap polymers, we tested the performance of these polymers by using them to disperse and select s-SWCNTs. Absorption spectroscopy is the most common and facile method to evaluate the quality of s-SWCNT/polymer inks. Figure 4a shows the absolute absorbance spectra of the polymer wrapped HiPCO-SWCNT inks after the first sonication and ultracentrifugation enrichment (see the Experimental Section). Dashed lines correspond to the spectra as obtained directly after first dispersal of the s-SWCNT. The solid lines are the spectra obtained for the enriched s-SWCNT inks, after two ultracentrifugation runs.⁵²

As discussed previously, the absorption peaks of PNDITEG-TVT and PNDIC8TEG-TVT are located from 500 to 1000 nm, which upon aggregation of the polymer chains exhibits distinct, additional features (see Figure S28). The narrow absorption peaks in the near-infrared region (1100–1700 nm) are evidence of the successful sorting of s-SWCNTs, corresponding to the first (S_{11}) electronic transitions of the different species present in the sample. These data confirm that PNDITEG-AH, PNDITEG-TVT, and PNDIC8TEG-TVT are able to discriminate and disperse s-SWCNTs selectively.

As expected, the S_{11} peaks are significantly enhanced after the enrichment procedure. From these intensities, it is clear that inks prepared using PNDIC8TEG-TVT yield the lowest density of s-SWCNT compared with PNDITEG-TVT and PNDITEG-AH in both discrimination-only and enriched inks. By contrast, there is little difference between the optical density of the s-SWCNTs obtained with PNDITEG-TVT and PNDITEG-AH, demonstrating the predicted effects of the vinylene moieties described above. We note that to be able to compare the absolute yields of s-SWCNT selected by each polymer directly we did not dilute the dispersion inks to an equal optical density.

To highlight the relative differences in yield with respect to the amount of polymer chains, we normalized the absorbance spectra to the free polymer peak (at 327 nm for PNDITEG-AH and 392–410 nm for PNDITEG-TVT and PNDIC8TEG-TVT), as shown in Figure 4b. Relative to this standard, PNDITEG-AH yields the highest amount of s-SWCNT after both the selection and enrichment steps. Comparing

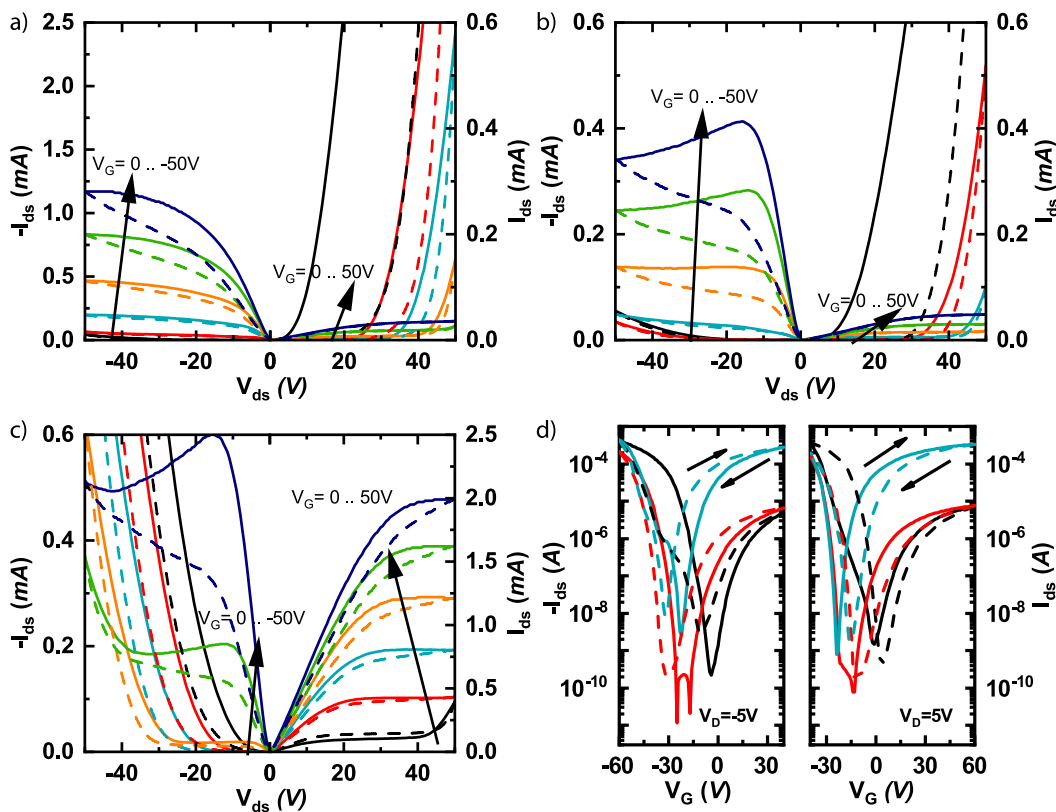


Figure 5. Comparison of electrical characteristics for the polymer wrapped s-SWCNT inks. (a–c) FET output characteristics for the examined inks for (a) a device fabricated from HiPCO:PNDITEG-AH (Adapted from our previous work⁴¹), (b) HiPCO:PNDITEG-TVT, and (c) HiPCO:PNDIC8TEG-TVT. The arrows represent an increase in gate bias from 0 to ± 50 V in steps of 10 V. (d) FET transfer characteristics for HiPCO:PNDITEG-AH (black), HiPCO:PNDITEG-TVT (red), and HiPCO:PNDIC8TEG-TVT (turquoise). The arrows represent the sweep directions.

PNDIC8TEG-TVT and PNDITEG-TVT, the first produces a smaller amount of s-SWCNTs for first sorted inks, as can be seen in the S_{11} (1100–1700 nm) region. However, interestingly, after the crucial enrichment step, a different trend emerges: The PNDIC8TEG-TVT sample yields a higher density of s-SWCNT, and the PNDITEG-TVT sample contains a lower amount of s-SWCNTs relative to free polymer. This indicates that it is more difficult to remove excess PNDITEG-TVT from the inks, resulting in a lower overall wrapping efficiency. The change in the ratio between the two polymer absorption peaks is significant, as the lower energy peak is indicative of aggregation on the SWCNT walls, while the high energy peak is a finger print of the free polymer chains.⁴⁰ In particular, after the second centrifugation, the low energy peak becomes more prominent, indicating that the polymer indeed is coiling around the s-SWCNT.

The absorption data demonstrate that the more planar polymers PNDITEG-TVT and PNDIC8TEG-TVT have a lower capability of dispersing (but not selecting for) s-SWCNT than the less planar PNDITEG-AH. The higher ability of PNDITEG-AH for dispersing s-SWCNT is likely a result of the twist in the head-to-head bithiophene moiety that favors a helical conformation for wrapping nanotubes.^{40,53–55} The minor difference between PNDITEG-AH and PNDITEG-TVT indicates that inserting a vinylene linker into PNDITEG-AH (thus forming PNDITEG-TVT) did not significantly sacrifice wrapping capability. Although the planar polymer PNDITEG-TVT is less prone to form a helical conformation to wrap s-SWCNT as compared with PNDITEG-AH, the

extended π -conjugation gives rise to a strong $\pi-\pi$ intermolecular interaction, which enhances $\pi-\pi$ interaction between the polymer chains and the s-SWCNT.^{24,37,38} Therefore, PNDITEG-TVT remains capable of wrapping the s-SWCNT, but the lower band gap compared to PNDITEG-AH should be beneficial to charge transport.

It has been demonstrated that the side chains are also very important for the wrapping of SWCNTs.⁵³ Therefore, since PNDITEG-TVT and PNDIC8TEG-TVT consist of the same π -conjugated backbone, the difference in dispersion yield should be a direct result from the variation in the side chain. Inserting an alkyl chain segment between the glycol side chain and backbone not only increases the solubility of the polymer but also reduces the polarity of PNDIC8TEG-TVT, which in turn results in a lower interaction with s-SWCNTs.^{23,24,27} Thus, PNDIC8TEG-TVT exhibits the lowest wrapping ability during selection. However, during the enrichment procedure, the excess (free) polymer in the supernatant is more easily removed in the case of PNDIC8TEG-TVT as compared with PNDITEG-TVT, which is likely due to the more flexible side chain of PNDIC8TEG-TVT, which increases its solubility. Since the polymers have a similar molecular weight and the amount used for preparing the solutions is kept constant, the total number of polymer chains within each solution is comparable.

In Figure 4c, the normalized steady-state photoluminescence (PL) spectra of the inks are shown. Using PNDITEG-AH as a reference, we can see that PNDITEG-TVT shows a slight preference for emission from high band gap SWCNTs. This is

in contrast with PNDIC8TEG-TVT, which shows slightly more intense emission at lower energies.

The small difference in intensity of the PL, considering that the absorption spectra of the three dispersions are almost identical, indicates subtle variation in the degree of energy transfer among SWCNTs of different chirality. This difference is further confirmed by time-resolved PL in Figure 4d, where the 1140 nm transition shows similar decay for all inks, with extracted lifetimes of $\tau_1 = 15$ ps (43%) and $\tau_2 = 39$ ps (57%). Since the lifetime is typically strongly quenched in the presence of metallic species and proximity with SWCNT of different chirality, the data indicate that the inks fabricated from the new polymers result in a similar degree of s-SWCNT individualization.⁵⁶ It is important to note that this is not always the case; we have previously demonstrated that in case of SWCNT wrapped with polythiophenes, the formation of twins is favored with strong consequences for the PL lifetime.⁵⁷

Thin-Film Transistor Performance. To evaluate the quality of the s-SWCNT:polymer inks and probe their charge transport properties, we fabricated bottom-gate and bottom-contact field-effect transistors (FETs). The enriched polymer sorted s-SWCNT inks were blade-cast onto the substrate with lithographically defined electrodes. Figure 5 displays the electrical characteristics of a representative set of FET devices made from the enriched polymer wrapped HiPCO s-SWCNT inks. There is a peculiar shift from p-type dominated toward more ambipolar, n-type dominated transport, going from HiPCO:PNDITEG-AH to HiPCO:PNDITEG-TVT to HiPCO:PNDIC8TEG-TVT. As shown in Figure 5a, the PNDITEG-AH-sorted s-SWCNT transistors exhibited p-dominated output characteristics. While in Figure 5b, HiPCO:PNDITEG-TVT-based FET still displayed p-dominated output characteristics, and slightly more electrons are present in the channel. In Figure 5c, the HiPCO:PNDIC8TEG-TVT-based FET displayed n-dominated output characteristics. The electron current for the HiPCO:PNDITEG-TVT device is almost 1 order of magnitude smaller as compared with HiPCO:PNDITEG-AH. Therefore, indicating that the electron-trapping mechanisms play relatively a more significant role in the transport properties, resulting in a larger relative hysteresis and eventually saturation (at about -15 V) of the channel current. The increased relative trapping together with charge carrier recombination can also explain the decrease of the current after saturation.

The p-type charge carrier dominated HiPCO:PNDITEG-AH ink exhibit the highest hole saturation current, while the HiPCO:PNDITEG-TVT and HiPCO:PNDIC8TEG-TVT inks exhibit similar hole current saturation. However, the electron current for the devices made from the enriched PNDIC8TEG-TVT-sorted s-SWCNT inks is 40 times larger in magnitude as compared with enriched PNDITEG-TVT-sorted s-SWCNT inks. Figure 5d shows the $I_D - V_G$ transfer characteristics of all three devices. The FETs obtained from PNDITEG-AH-sorted s-SWCNT exhibit a hole mobility of $0.82 \text{ cm}^2 \text{ V}^{-1} \text{ s}^{-1}$ (on-off ratio $\approx 9 \times 10^6$) and an electron mobility of $0.02 \text{ cm}^2 \text{ V}^{-1} \text{ s}^{-1}$ (on-off ratio $\approx 8 \times 10^3$). The FETs obtained from PNDITEG-TVT-sorted s-SWCNT exhibit a hole mobility of $1.52 \text{ cm}^2 \text{ V}^{-1} \text{ s}^{-1}$ (on-off ratio 2×10^7) and an electron mobility of $0.05 \text{ cm}^2 \text{ V}^{-1} \text{ s}^{-1}$ (on-off ratio 5×10^5). The FETs obtained from PNDIC8TEG-TVT-sorted s-SWCNT exhibit ambipolar characteristics with a hole mobility of $2.31 \text{ cm}^2 \text{ V}^{-1} \text{ s}^{-1}$ (on-off ratio 2×10^6) and an electron mobility of $0.38 \text{ cm}^2 \text{ V}^{-1} \text{ s}^{-1}$ (on-off ratio 2×10^6).

A summary of the FET performance distribution in devices fabricated with these enriched polymer-sorted s-SWCNT inks is reported in Figure 6. It is clear that HiPCO:PNDITEG-AH-

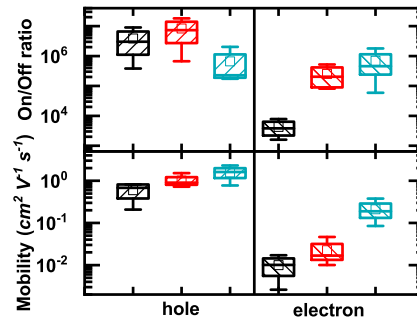


Figure 6. Figures of merit of the FETs fabricated from HiPCO:PNDITEG-AH (black), HiPCO:PNDITEG-TVT (red), and HiPCO:PNDIC8TEG-TVT (turquoise) inks.

based FETs demonstrate the lowest performance as compared with that of HiPCO:PNDITEG-TVT- and HiPCO:PNDIC8TEG-TVT-based FETs in both hole and electron mobility, despite the fact that PNDITEG-AH exhibits the highest dispersion capability as indicated by the absorption spectra. In contrast with the absorption spectra, the FET data give a clear indication that there are no metallic tubes present in the devices. All transistors were functional and the hole on-off ratios is in the order of 10^6 or above.

Energy Level Alignment and FET Hysteresis. As described above, the FET performances can be affected by the energy levels and mobility of polymers. Figure 7 shows the energy level alignment of the three investigated polymers and the (8,7) s-SWCNT. Compared with PNDITEG-AH, the higher HOMO level of vinylene-containing polymers PNDITEG-TVT and PNDIC8TEG-TVT result in an improved energy alignment with the HOMO levels of the s-SWCNT. Therefore, the energy barrier for intertube hole transport in a network for NDI-TVT based polymer-wrapped s-SWCNT is lower than that of NDI-AH based polymer-wrapped s-SWCNT. In the case of electron transport, these three polymers show energy alignment similar to that of (8,7) s-SWCNT. However, as compared with previously reported NDI-TVT-based polymers, the electron mobility of PNDITEG-AH is expected to be lower.^{45,47,58} This can be explained by the more twisted backbone of PNDITEG-AH. This lower electron mobility within the polymer results in a higher energy barrier for electron transport from one s-SWCNT to another, reducing overall FET electron mobilities.

The devices made from the HiPCO:PNDIC8TEG-TVT ink display higher mobilities as compared to PNDITEG-TVT, for both hole and electron conduction. Combining these data with the absorption spectra, we suspect this improvement is likely due to a higher polymer dispersion efficiency, i.e., more s-SWCNT are selected with respect to the remaining free polymer in the ink after purification. The lower amount of free polymer significantly reduces the barrier between the s-SWCNT for intratube charge transport, resulting in the higher FET performances seen for PNDIC8TEG-TVT as compared with that of PNDITEG-TVT. Other data supporting this hypothesis include that FET devices fabricated immediately after selection (before enrichment) using the PNDITEG-TVT s-SWCNT ink show 100 times higher hole mobility than that of PNDIC8TEG-TVT. After enrichment, the excess polymer

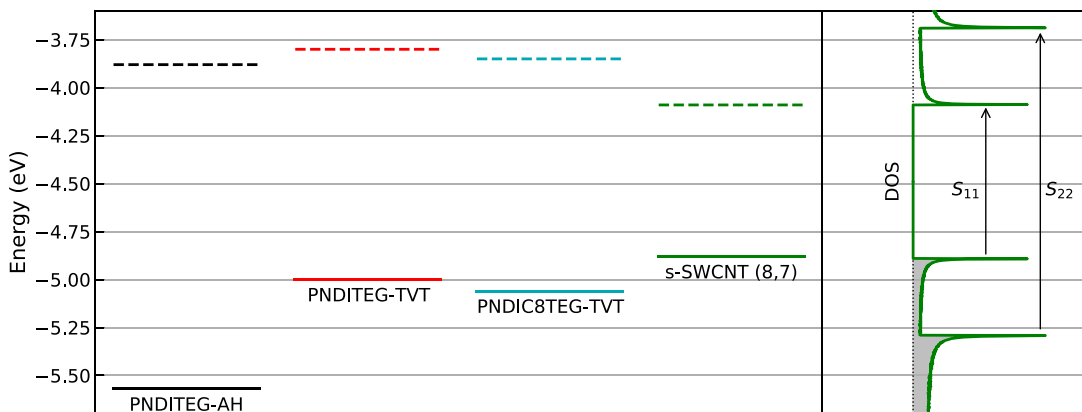


Figure 7. Energy levels (solid for HOMO, dashed for LUMO) of PNDITEG-AH, PNDITEG-TVT, and PNDIC8TEG-TVT compared with s-SWCNT (8,7). On the diagram on the right is displayed the density of states for the (8,7) s-SWCNT schematically represented. The s-SWCNT data for HOMO and LUMO are taken from ref 59.

is removed, and the PNDIC8TEG-TVT solution is still superior over PNDITEG-TVT. Additionally, PNDIC8TEG-TVT-based FET displays more ambipolar electrical characteristics than PNDITEG-TVT-based FETs. The electron mobility of the PNDIC8TEG-TVT-based FET is only 1 order of magnitude lower in hole mobility. Interestingly, the increase of ambipolarity in this sample slightly degrades the hole on–off ratio of the device, giving values above 10^5 . This is also reflected by statistics over all devices (Figure 6 and Table S3). We note that ambipolarity in a FET for many applications is undesirable; however, polarity tuning through the use of dopants has previously been demonstrated as a potential solution.⁵

To further help clarify the role of the wrapping polymer, the FET hysteresis is examined. The hysteresis was quantified by taking the difference in threshold voltage (V_{th}) between forward and backward sweep, as obtained during the transfer characteristics measurements (summarized in Table S3). Interestingly, the hysteresis for holes in HiPCO:PNDITEG-AH is significantly larger than the value as obtained for HiPCO:PNDITEG-TVT or HiPCO:PNDIC8TEG-TVT. This can be explained by the higher energetic barrier of PNDITEG-AH, which enhances the possibility of trapping. In contrast, the hysteresis for electron transport is slightly lower for HiPCO:PNDITEG-AH, although similar to the one of the other two polymers. Indeed, the LUMO of this particular polymer lies slightly closer to that of the s-SWCNT, as compared with PNDITEG-TVT and PNDIC8TEG-TVT (Figure 7). These data support our hypothesis that the energy levels of PNDITEG-TVT and PNDIC8TEG-TVT are better aligned with the s-SWCNT, reducing the energy barrier for holes and improving charge transport.

Overall, the HiPCO:SWCNT dispersions (obtained with PNDITEG-AH, PNDITEG-TVT, and PNDIC8TEG-TVT) are of very good quality and demonstrate that small variations of the chemical structure of the wrapping polymer can have a large influence on the transport properties of the inks.

CONCLUSION

We have successfully demonstrated that two newly synthesized naphthalene diimide based narrow-band-gap conjugated polymers are able to wrap and select semiconducting SWCNT. Compared to the conjugated polymers with naphthalene diimide and head-to-head bithiophene units

(PNDITEG-AH), we found that inserting a small conjugated vinyl group into the head-to-head bithiophene substantially increases backbone planarity and lowers the band gap of the corresponding conjugated polymers (PNDITEG-TVT and PNDIC8TEG-TVT) without sacrificing the wrapping ability significantly. Furthermore, usage of an alkyl chain spacer between conjugated backbone and oligomer glycol ether side chain increases the flexibility and solubility of PNDIC8TEG-TVT, which leads to efficient removal of excess polymer from the s-SWCNT ink during the enrichment step. Field-effect transistors fabricated from PNDITEG-AH-, PNDITEG-TVT-, and PNDIC8TEG-TVT-wrapped s-SWCNT were fabricated and used as a tool to evaluate the influence of the backbone on the device performance. The hole transport of devices fabricated with PNDITEG-AH, PNDITEG-TVT, and PNDIC8TEG-TVT selected s-SWCNT increased gradually from twisted polymers PNDITEG-AH to planar polymers PNDITEG-TVT and PNDIC8TEG-TVT. The higher performance of PNDITEG-TVT and PNDIC8TEG-TVT originate from their improved HOMO level alignment with nanotubes, as compared with that of PNDITEG-AH. Our work provides insight into the fundamental understanding of the relationship between the molecular structure of the polymer and corresponding dispersion capability of SWCNT and physical properties of the final inks.

EXPERIMENTAL SECTION

Preparation and Characterization of s-SWCNT Dispersions. HiPCO SWCNT (0.8 nm 1.2 nm) inks and devices were prepared and characterized as described in our previous work.⁶⁰ FET performances (per ink) are based on multiple transistors residing on a chip, for multiple chips. A detailed description of the characterization of the inks and fabrication of the transistors is available in the Supporting Information.

DFT Calculations. DFT calculations were performed using Gaussian 16 program with B3LYP functional and 6-311G(d) basis set. We choose one repeat unit of each polymer as the model molecule in our simulation to reduce the calculation time. These model molecules were first optimized at gas phase. Then we used the optimized geometry as the starting point for further single point energy calculations.

ASSOCIATED CONTENT

Supporting Information

The Supporting Information is available free of charge at <https://pubs.acs.org/doi/10.1021/acsami.2c07158>.

Detailed description of the synthesis and characterization of the materials; NMR and FT-IR spectra; Mal迪TOF-MS spectra; TGA and DSC curves; DFT calculation; preparation and characterization of SWCNT dispersions; UV-vis-NIR spectra; transistor device fabrication and measurement; AFM images and other data ([PDF](#))

AUTHOR INFORMATION

Corresponding Authors

Gang Ye — Zernike Institute for Advanced Materials, University of Groningen, 9747 AG Groningen, The Netherlands; Center for Biomedical Optics and Photonics (CBOP) & College of Physics and Optoelectronic Engineering, Key Laboratory of Optoelectronic Devices and Systems, Shenzhen University, Shenzhen 518060, PR China; Stratingh Institute for Chemistry, University of Groningen, 9747 AG Groningen, The Netherlands; Present Address: State Key Laboratory of Polymer Physics and Chemistry, Changchun Institute of Applied Chemistry, Chinese Academy of Sciences, Changchun, 130022 Jilin, PR China; Email: g.ye0612@ciac.ac.cn

Ryan C. Chiechi — Stratingh Institute for Chemistry, University of Groningen, 9747 AG Groningen, The Netherlands; Department of Chemistry and Carbon Electronics Cluster, North Carolina State University, Raleigh, North Carolina 27695-8204, United States;  [orcid.org/0000-0002-0895-2095](#); Email: ryan.chiechi@ncsu.edu

Maria Antonietta Loi — Zernike Institute for Advanced Materials, University of Groningen, 9747 AG Groningen, The Netherlands;  [orcid.org/0000-0002-7985-7431](#); Email: m.a.loi@rug.nl

Authors

Wytse Talsma — Zernike Institute for Advanced Materials, University of Groningen, 9747 AG Groningen, The Netherlands;  [orcid.org/0000-0003-3618-4393](#)

Yuru Liu — Zernike Institute for Advanced Materials, University of Groningen, 9747 AG Groningen, The Netherlands; Stratingh Institute for Chemistry, University of Groningen, 9747 AG Groningen, The Netherlands

Herman Duim — Zernike Institute for Advanced Materials, University of Groningen, 9747 AG Groningen, The Netherlands

Sietske Dijkstra — Zernike Institute for Advanced Materials, University of Groningen, 9747 AG Groningen, The Netherlands

Karolina Tran — Zernike Institute for Advanced Materials, University of Groningen, 9747 AG Groningen, The Netherlands

Junle Qu — Center for Biomedical Optics and Photonics (CBOP) & College of Physics and Optoelectronic Engineering, Key Laboratory of Optoelectronic Devices and Systems, Shenzhen University, Shenzhen 518060, PR China

Jun Song — Center for Biomedical Optics and Photonics (CBOP) & College of Physics and Optoelectronic Engineering, Key Laboratory of Optoelectronic Devices and Systems, Shenzhen University, Shenzhen 518060, PR China;  [orcid.org/0000-0002-2321-7064](#)

Complete contact information is available at:
<https://pubs.acs.org/10.1021/acsami.2c07158>

Author Contributions

W.T. and G.Y. contributed equally to this work.

Notes

The authors declare no competing financial interest.

ACKNOWLEDGMENTS

This work has been partially supported by the National Natural Science Foundation of China (61620106016, 61835009, and 61775145) and the Shenzhen Basic Research Program (JCYJ20210324095810028 and JCYJ20190808160207366). G.Y. acknowledges the China Postdoctoral Science Foundation Funded Project (grant 2020M672771) and Guangdong Basic and Applied Basic Research Foundation (2020A1515110636). The authors are thankful to A. Kamp and T. Zaharia for technical support. The authors thank the Zernike Institute for Advanced Materials for financial support that was vital in completing this research. Y.L. acknowledges financial support from the China Scholarship Council. We thank the Center for Information Technology of the University of Groningen for their support and for providing access to the Peregrine high-performance computing cluster.

REFERENCES

- (1) Derenskyi, V.; Gomulya, W.; Rios, J. M. S.; Fritsch, M.; Fröhlich, N.; Jung, S.; Allard, S.; Bisri, S. Z.; Gordiichuk, P.; Herrmann, A.; Scherf, U.; Loi, M. A. Carbon Nanotube Network Ambipolar Field-Effect Transistors with 108 On/Off Ratio. *Adv. Mater.* **2014**, *26*, 5969–5975.
- (2) Bisri, S. Z.; Derenskyi, V.; Gomulya, W.; Salazar-Rios, J. M.; Fritsch, M.; Fröhlich, N.; Jung, S.; Allard, S.; Scherf, U.; Loi, M. A. Anomalous Carrier Transport in Ambipolar Field-Effect Transistor of Large Diameter Single-Walled Carbon Nanotube Network. *Advanced Electronic Materials* **2016**, *2*, 1500222.
- (3) Schießl, S. P.; Fröhlich, N.; Held, M.; Gannott, F.; Schweiger, M.; Forster, M.; Scherf, U.; Zaumseil, J. Polymer-sorted semiconducting carbon nanotube networks for high-performance ambipolar field-effect transistors. *ACS Appl. Mater. Interfaces* **2015**, *7*, 682–689.
- (4) Derenskyi, V.; Gomulya, W.; Talsma, W.; Salazar-Rios, J. M.; Fritsch, M.; Nirmalraj, P.; Riel, H.; Allard, S.; Scherf, U.; Loi, M. A. On-Chip Chemical Self-Assembly of Semiconducting Single-Walled Carbon Nanotubes (SWNTs): Toward Robust and Scale Invariant SWNTs Transistors. *Adv. Mater.* **2017**, *29*, 1606757.
- (5) Salazar-Rios, J. M.; Sengrian, A. A.; Talsma, W.; Duim, H.; Abdu-Aguye, M.; Jung, S.; Fröhlich, N.; Allard, S.; Scherf, U.; Loi, M. A. Customizing the Polarity of Single-Walled Carbon-Nanotube Field-Effect Transistors Using Solution-Based Additives. *Advanced Electronic Materials* **2020**, *6*, 1900789.
- (6) Sun, D.-M.; Timmermans, M. Y.; Kaskela, A.; Nasibulin, A. G.; Kishimoto, S.; Mizutani, T.; Kauppinen, E. I.; Ohno, Y. Mouldable all-carbon integrated circuits. *Nat. Commun.* **2013**, *4*, 2302.
- (7) Yang, Y.; Ding, L.; Han, J.; Zhang, Z.; Peng, L. M. High-Performance Complementary Transistors and Medium-Scale Integrated Circuits Based on Carbon Nanotube Thin Films. *ACS Nano* **2017**, *11*, 4124–4132.
- (8) Lee, S. Y.; Lee, S. W.; Kim, S. M.; Yu, W. J.; Jo, Y. W.; Lee, Y. H. Scalable complementary logic gates with chemically doped semiconducting carbon nanotube transistors. *ACS Nano* **2011**, *5*, 2369–2375.
- (9) Yang, Y.; Ding, L.; Chen, H.; Han, J.; Zhang, Z.; Peng, L. M. Carbon nanotube network film-based ring oscillators with sub 10-ns propagation time and their applications in radio-frequency signal transmission. *Nano Research* **2018**, *11*, 300–310.
- (10) Park, J.; Lee, Y.; Choi, B.; Yoon, J.; Kim, Y.; Kim, H. J.; Kang, M. H.; Kim, D. H.; Kim, D. M.; Choi, S. J. Directly drawn top-gate

- semiconducting carbon nanotube thin-film transistors and complementary inverters. *Nanotechnology* **2020**, *31*, 32LT01.
- (11) Scuratti, F.; Bonacchini, G. E.; Bossio, C.; Salazar-Rios, J. M.; Talsma, W.; Loi, M. A.; Antognazza, M. R.; Caironi, M. Real-Time Monitoring of Cellular Cultures with Electrolyte-Gated Carbon Nanotube Transistors. *ACS Appl. Mater. Interfaces* **2019**, *11*, 37966–37972.
- (12) Cardenas, J. A.; Andrews, J. B.; Noyce, S. G.; Franklin, A. D. Carbon nanotube electronics for IoT sensors. *Nano Futures* **2020**, *4*, 012001.
- (13) Wang, C.; Chien, J.-C.; Takei, K.; Takahashi, T.; Nah, J.; Niknejad, A. M.; Javey, A. Extremely Bendable, High-Performance Integrated Circuits Using Semiconducting Carbon Nanotube Networks for Digital, Analog, and Radio-Frequency Applications. *Nano Lett.* **2012**, *12*, 1527–1533.
- (14) Zhang, H.; Xiang, L.; Yang, Y.; Xiao, M.; Han, J.; Ding, L.; Zhang, Z.; Hu, Y.; Peng, L. M. High-Performance Carbon Nanotube Complementary Electronics and Integrated Sensor Systems on Ultrathin Plastic Foil. *ACS Nano* **2018**, *12*, 2773–2779.
- (15) Lei, T.; Shao, L. L.; Zheng, Y. Q.; Pitner, G.; Fang, G.; Zhu, C.; Li, S.; Beausoleil, R.; Wong, H. S.; Huang, T. C.; et al. Low-voltage high-performance flexible digital and analog circuits based on ultrahigh-purity semiconducting carbon nanotubes. *Nat. Commun.* **2019**, *10*, 2161.
- (16) Shulaker, M. M.; Hills, G.; Patil, N.; Wei, H.; Chen, H. Y.; Wong, H. S.; Mitra, S. Carbon nanotube computer. *Nature* **2013**, *501*, S26–S30.
- (17) Hills, G.; Lau, C.; Wright, A.; Fuller, S.; Bishop, M. D.; Srimani, T.; Kanhaiya, P.; Ho, R.; Amer, A.; Stein, Y.; Murphy, D.; Arvind; Chandrasekaran, A.; Shulaker, M. M. Modern microprocessor built from complementary carbon nanotube transistors. *Nature* **2019**, *572*, 595–602.
- (18) Park, S.; Vosguerichian, M.; Bao, Z. A review of fabrication and applications of carbon nanotube film-based flexible electronics. *Nanoscale* **2013**, *5*, 1727.
- (19) De Volder, M. F.; Tawfick, S. H.; Baughman, R. H.; Hart, A. J. Carbon nanotubes: Present and future commercial applications. *Science* **2013**, *339*, 535–539.
- (20) Wan, H.; Cao, Y.; Lo, L. W.; Zhao, J.; Sepúlveda, N.; Wang, C. Flexible Carbon Nanotube Synaptic Transistor for Neurological Electronic Skin Applications. *ACS Nano* **2020**, *14*, 10402–10412.
- (21) He, M.; Zhang, S.; Zhang, J. Horizontal Single-Walled Carbon Nanotube Arrays: Controlled Synthesis, Characterizations, and Applications. *Chem. Rev.* **2020**, *120*, 12592–12684.
- (22) Samanta, S. K.; Fritsch, M.; Scherf, U.; Gomulya, W.; Bisri, S. Z.; Loi, M. A. Conjugated polymer-Assisted dispersion of single-wall carbon nanotubes: The power of polymer wrapping. *Acc. Chem. Res.* **2014**, *47*, 2446–2456.
- (23) Lei, T.; Pochorovski, I.; Bao, Z. Separation of Semiconducting Carbon Nanotubes for Flexible and Stretchable Electronics Using Polymer Removable Method. *Acc. Chem. Res.* **2017**, *50*, 1096–1104.
- (24) Wang, J.; Lei, T. Separation of Semiconducting Carbon Nanotubes Using Conjugated Polymer Wrapping. *Polymers* **2020**, *12*, 1548.
- (25) Qiu, C.; Zhang, Z.; Xiao, M.; Yang, Y.; Zhong, D.; Peng, L. M. Scaling carbon nanotube complementary transistors to 5-nm gate lengths. *Science* **2017**, *355*, 271–276.
- (26) Baughman, R. H.; Zakhidov, A. A.; De Heer, W. A. Carbon nanotubes - The route toward applications. *Science* **2002**, *297*, 787–792.
- (27) Fong, D.; Adronov, A. Recent developments in the selective dispersion of single-walled carbon nanotubes using conjugated polymers. *Chemical Science* **2017**, *8*, 7292–7305.
- (28) Arnold, M. S.; Green, A. A.; Hulvat, J. F.; Stupp, S. I.; Hersam, M. C. Sorting carbon nanotubes by electronic structure using density differentiation. *Nature Nanotechnol.* **2006**, *1*, 60–65.
- (29) Miyata, Y.; Shiozawa, K.; Asada, Y.; Ohno, Y.; Kitaura, R.; Mizutani, T.; Shinohara, H. Length-sorted semiconducting carbon nanotubes for high-mobility thin film transistors. *Nano Research* **2011**, *4*, 963–970.
- (30) Nish, A.; Hwang, J.-Y.; Doig, J.; Nicholas, R. J. Highly selective dispersion of single-walled carbon nanotubes using aromatic polymers. *Nat. Nanotechnol.* **2007**, *2*, 640–646.
- (31) Rice, N. A.; Bodnaryk, W. J.; Mirka, B.; Melville, O. A.; Adronov, A.; Lessard, B. H. Polycarbazole-Sorted Semiconducting Single-Walled Carbon Nanotubes for Incorporation into Organic Thin Film Transistors. *Advanced Electronic Materials* **2019**, *5*, 1800539.
- (32) Boudreault, P. L. T.; Beaupré, S.; Leclerc, M. Polycarbazoles for plastic electronics. *Polym. Chem.* **2010**, *1*, 127–136.
- (33) Lemasson, F. A.; Strunk, T.; Gerstel, P.; Hennrich, F.; Lebedkin, S.; Barner-Kowollik, C.; Wenzel, W.; Kappes, M. M.; Mayor, M. Selective dispersion of single-walled carbon nanotubes with specific chiral indices by poly(N-decyl-2,7-carbazole). *J. Am. Chem. Soc.* **2011**, *133*, 652–655.
- (34) Lee, H. W.; Yoon, Y.; Park, S.; Oh, J. H.; Hong, S.; Liyanage, L. S.; Wang, H.; Morishita, S.; Patil, N.; Park, Y. J.; et al. Selective dispersion of high purity semiconducting single-walled carbon nanotubes with regioregular poly(3-alkylthiophene)s. *Nat. Commun.* **2011**, *2*, 541.
- (35) Lee, M.-H.; Lee, S.-H.; Kim, J.; Lee, S. Y.; Lim, D.-H.; Hwang, K.; Hwang, H.; Jung, Y. C.; Noh, Y.-Y.; Kim, D.-Y. Selective sorting of semiconducting single-walled carbon nanotubes using thiénylenevinylen-based conjugated polymers with high alkyl side-chain density. *Carbon* **2017**, *125*, 571–581.
- (36) Gomulya, W.; Derenskyi, V.; Kozma, E.; Pasini, M.; Loi, M. A. Polyazazines and Polyazomethines with Didodecylthiophene Units for Selective Dispersion of Semiconducting Single-Walled Carbon Nanotubes. *Adv. Funct. Mater.* **2015**, *25*, 5858–5864.
- (37) Lei, T.; Lai, Y. C.; Hong, G.; Wang, H.; Hayoz, P.; Weitz, R. T.; Chen, C.; Dai, H.; Bao, Z. (DPP) Diketopyrrolopyrrole-Based Donor-Acceptor Polymers for Selective Dispersion of Large-Diameter Semiconducting Carbon Nanotubes. *Small* **2015**, *11*, 2946–2954.
- (38) Lei, T.; Pitner, G.; Chen, X.; Hong, G.; Park, S.; Hayoz, P.; Weitz, R. T.; Wong, H. S. P.; Bao, Z. Dispersion of High-Purity Semiconducting Arc-Discharged Carbon Nanotubes Using Backbone Engineered Diketopyrrolopyrrole (DPP)-Based Polymers. *Advanced Electronic Materials* **2016**, *2*, 1500299.
- (39) Salazar-Rios, J. M.; Gomulya, W.; Derenskyi, V.; Yang, J.; Bisri, S. Z.; Chen, Z.; Faccetti, A.; Loi, M. A. Selecting Semiconducting Single-Walled Carbon Nanotubes with Narrow Bandgap Naphthalene Diimide-Based Polymers. *Advanced Electronic Materials* **2015**, *1*, 1500074.
- (40) Salazar-Rios, J. M.; Talsma, W.; Derenskyi, V.; Gomulya, W.; Keller, T.; Fritsch, M.; Kowalski, S.; Preis, E.; Wang, M.; Allard, S.; et al. Understanding the Selection Mechanism of the Polymer Wrapping Technique toward Semiconducting Carbon Nanotubes. *Small Methods* **2018**, *2*, 1700335.
- (41) Ye, G.; Talsma, W.; Tran, K.; Liu, Y.; Dijkstra, S.; Cao, J.; Chen, J.; Qu, J.; Song, J.; Loi, M. A.; Chiechi, R. C. Polar Side Chains Enhance Selection of Semiconducting Single-Walled Carbon Nanotubes by Polymer Wrapping. *Macromolecules* **2022**, *55*, 1386–1397.
- (42) Guo, X.; Watson, M. D. Conjugated Polymers from Naphthalene Bisimide. *Org. Lett.* **2008**, *10*, 5333–5336.
- (43) Higginbotham, H. F.; Maniam, S.; Langford, S. J.; Bell, T. D. New brightly coloured, water soluble, core-substituted naphthalene diimides for biophysical applications. *Dyes Pigm.* **2015**, *112*, 290–297.
- (44) Kim, R.; Kang, B.; Sin, D. H.; Choi, H. H.; Kwon, S.-K.; Kim, Y.-H.; Cho, K. Oligo (ethylene glycol)-incorporated hybrid linear alkyl side chains for n-channel polymer semiconductors and their effect on the thin-film crystalline structure. *Chem. Commun.* **2015**, *51*, 1524–1527.
- (45) Kim, R.; Amegadze, P. S.; Kang, I.; Yun, H. J.; Noh, Y. Y.; Kwon, S. K.; Kim, Y. H. High-mobility air-stable naphthalene diimide-based copolymer containing extended π-conjugation for n-channel organic field effect transistors. *Adv. Funct. Mater.* **2013**, *23*, 5719–5727.

- (46) Choi, J.; Kim, K. H.; Yu, H.; Lee, C.; Kang, H.; Song, I.; Kim, Y.; Oh, J. H.; Kim, B. J. Importance of Electron Transport Ability in Naphthalene Diimide-Based Polymer Acceptors for High-Performance, Additive-Free, All-Polymer Solar Cells. *Chem. Mater.* **2015**, *27*, 5230–5237.
- (47) Chen, H.; Guo, Y.; Mao, Z.; Yu, G.; Huang, J.; Zhao, Y.; Liu, Y. Naphthalenediimide-based copolymers incorporating vinyl-linkages for high-performance ambipolar field-effect transistors and complementary-like inverters under air. *Chem. Mater.* **2013**, *25*, 3589–3596.
- (48) Zhang, L.; Rose, B. D.; Liu, Y.; Nahid, M. M.; Gann, E.; Ly, J.; Zhao, W.; Rosa, S. J.; Russell, T. P.; Facchetti, A.; McNeill, C. R.; Brédas, J. L.; Briseno, A. L. Efficient Naphthalenediimide-Based Hole Semiconducting Polymer with Vinylene Linkers between Donor and Acceptor Units. *Chem. Mater.* **2016**, *28*, 8580–8590.
- (49) Hay, M.; Klavetter, F. L. Aliphatic Phenylene Vinylene Copolymers: Tuning the Color of Luminescence through Comonomer Feed Ratios. *J. Am. Chem. Soc.* **1995**, *117*, 7112–7118.
- (50) Li, J.; Yan, M.; Xie, Y.; Qiao, Q. Linker effects on optoelectronic properties of alternate donor-acceptor conjugated polymers. *Energy Environ. Sci.* **2011**, *4*, 4276–4283.
- (51) Frisch, M. J.; Trucks, G. W.; Schlegel, H. B.; Scuseria, G. E.; Robb, M. A.; Cheeseman, J. R.; Scalmani, G.; Barone, V.; Petersson, G. A.; Nakatsuji, H.; Li, X.; Caricato, M.; Marenich, A. V.; Bloino, J.; Janesko, B. G.; Gomperts, R.; Mennucci, B.; Hratchian, H. P.; Ortiz, J. V.; Izmaylov, A. F.; Sonnenberg, J. L.; Williams-Young, D.; Ding, F.; Lipparini, F.; Egidi, F.; Goings, J.; Peng, B.; Petrone, A.; Henderson, T.; Ranasinghe, D.; Zakrzewski, V. G.; Gao, J.; Rega, N.; Zheng, G.; Liang, W.; Hada, M.; Ehara, M.; Toyota, K.; Fukuda, R.; Hasegawa, J.; Ishida, M.; Nakajima, T.; Honda, Y.; Kitao, O.; Nakai, H.; Vreven, T.; Throssell, K.; Montgomery, J. A., Jr.; Peralta, J. E.; Ogliaro, F.; Bearpark, M.; Heyd, J. J.; Brothers, E. N.; Kudin, K. N.; Staroverov, V. N.; Kobayashi, R.; Normand, J.; Raghavachari, K.; Rendell, A.; Burant, J. C.; Iyengar, S. S.; Tomasi, J.; Cossi, M.; Millam, J. M.; Klene, M.; Adamo, C.; Cammi, R.; Ochterski, J. W.; Martin, R. L.; Morokuma, K.; Farkas, O.; Foresman, J. B.; Fox, D. J. *Gaussian 16*, revision C.01; Gaussian, Inc.: Wallingford, CT, 2016.
- (52) Bisri, S. Z.; Gao, J.; Derenskyi, V.; Gomulya, W.; Iezhokin, I.; Gordiichuk, P.; Herrmann, A.; Loi, M. A. High Performance Ambipolar Field-Effect Transistor of Random Network Carbon Nanotubes. *Adv. Mater.* **2012**, *24*, 6147–6152.
- (53) Gomulya, W.; Costanzo, G. D.; de Carvalho, E. J. F.; Bisri, S. Z.; Derenskyi, V.; Fritsch, M.; Fröhlich, N.; Allard, S.; Gordiichuk, P.; Herrmann, A.; Marrink, S. J.; dos Santos, M. C.; Scherf, U.; Loi, M. A. Semiconducting single-walled carbon nanotubes on demand by polymer wrapping. *Adv. Mater.* **2013**, *25*, 2948–2956.
- (54) Gao, J.; Loi, M. A.; de Carvalho, E. J. F.; dos Santos, M. C. Selective Wrapping and Supramolecular Structures of Polyfluorene-Carbon Nanotube Hybrids. *ACS Nano* **2011**, *5*, 3993–3999.
- (55) Nirmalraj, P.; dos Santos, M. C.; Salazar Rios, J. M.; Davila, D.; Vargas, F.; Scherf, U.; Loi, M. A. Polymer–Nanocarbon Topological and Electronic Interface. *Langmuir* **2018**, *34*, 6225–6230.
- (56) Gao, J.; Kwak, M.; Wildeman, J.; Herrmann, A.; Loi, M. A. Effectiveness of sorting single-walled carbon nanotubes by diameter using polyfluorene derivatives. *Carbon* **2011**, *49*, 333–338.
- (57) Gomulya, W.; Salazar Rios, J. M.; Derenskyi, V.; Bisri, S. Z.; Jung, S.; Fritsch, M.; Allard, S.; Scherf, U.; dos Santos, M. C.; Loi, M. A. Effect of temperature on the selection of semiconducting single walled carbon nanotubes using Poly(3-dodecylthiophene-2,5-diyl). *Carbon* **2015**, *84*, 66–73.
- (58) Guo, X.; Kim, F. S.; Seger, M. J.; Jenekhe, S. A.; Watson, M. D. Naphthalene diimide-based polymer semiconductors: synthesis, structure–property correlations, and n-channel and ambipolar field-effect transistors. *Chem. Mater.* **2012**, *24*, 1434–1442.
- (59) Tanaka, Y.; Hirana, Y.; Niidome, Y.; Kato, K.; Saito, S.; Nakashima, N. Experimentally determined redox potentials of individual (n,m) single-walled carbon nanotubes. *Angewandte Chemie - International Edition* **2009**, *48*, 7655–7659.
- (60) Talsma, W.; Sengrian, A. A.; Salazar-Rios, J. M.; Duim, H.; Abdu-Aguye, M.; Jung, S.; Allard, S.; Scherf, U.; Loi, M. A.

Remarkably Stable, High-Quality Semiconducting Single-Walled Carbon Nanotube Inks for Highly Reproducible Field-Effect Transistors. *Advanced Electronic Materials* **2019**, *5*, 1900288.

□ Recommended by ACS

Use of a Multiple Hydride Donor To Achieve an n-Doped Polymer with High Solvent Resistance

Farzaneh Saeedifard, Seth R. Marder, et al.

JULY 13, 2022

ACS APPLIED MATERIALS & INTERFACES

READ ▶

All-Polymer Photodetectors with n-Type Polymers Having Nonconjugated Spacers for Dark Current Density Reduction

Hyeokjun Kim, In Hwan Jung, et al.

OCTOBER 17, 2022

MACROMOLECULES

READ ▶

Stretchable N-Type High-Performance Polymers Based on Asymmetric Thienylvinyl-1,1-Dicyanomethylene-3-Indanone for Plastic Electronics

Yongjoon Cho, Changduk Yang, et al.

JANUARY 31, 2022

CHEMISTRY OF MATERIALS

READ ▶

Structural Engineering of Anthracene Diimide Polymers for Molecular Ordering Manipulation

Dandan Tu, Can Li, et al.

MAY 05, 2022

MACROMOLECULES

READ ▶

Get More Suggestions >